Broadband Active Noise Control Around Human's Head - Determination and Achievement of Physical Limits

T. Kletschkowski[1], D. Sachau[1]

[1] *Helmut-Schmidt-University/University of the Federal Armed Forces Hamburg,Germany,*
Email: thomas.kletschkowski@hsuhh.de, sachau@hsuhh.de

Abstract

In order to prevent serious diseases caused by continuous noise pollution and to guarantee a restorative sleep the concept of active noise control (ANC) was applied to bedrooms. To determine the physical limits of this concept in a particular situation a transmission test rig was used to simulate real world conditions. A conventional bed (placed in the reverberation room) with a dummy head microphone was used to model the sleeping person. Two error microphones (inside the pillow) were used for multi-channel feed-forward control. The reference microphone was placed in front of a tilted window that was mounted into the transmission path. At first the physical limits of the control profit were determined by coherence-analysis. Then a proper filter length was calculated by quadratic optimization in time domain. This procedure was based on measured impulse response functions. Finally the noise reductions at the error microphones were determined for broadband disturbances 80 Hz $< f <$ 480 Hz. It turned out that the control profit of up to 18 dB was equivalent to the noise reduction predicted by coherence-analysis.

Description of Test Rig

The plant in which disturbing noise has to be reduced will in practice be given by a bed room with an open window. This situation was simulated using a transmission test rig that consists of an anechoic chamber and a reverberation room (with mean reverberation time of 0.64 s).

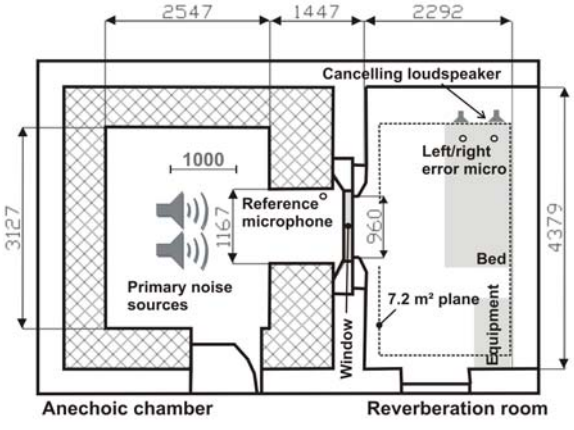

Figure 1: Dimension of transmission test rig used for experimental analysis of an active noise control system with one reference microphone, two error microphones and two cancelling loudspeakers

As shown in Figure 1, acoustic coupling was realized by a tilted window. Primary noise was generated in the anechoic chamber using four electro-dynamical loudspeakers (Type: PAB 515/BL).

The reference signal was measured in the anechoic chamber using a microphone (Type: B&K 4188). Two microphones of the same type were used to measure the error signals. The anti-noise was generated by two cancelling loudspeakers (Type: Genelec 8020). A multi channel FFT-analyzer (Type: OnoSokki DS-2000) and analogue filters (Type: Kemo VBF21) were used to prevent aliasing and imaging, respectively. The experimental setup is shown in Figure 2.

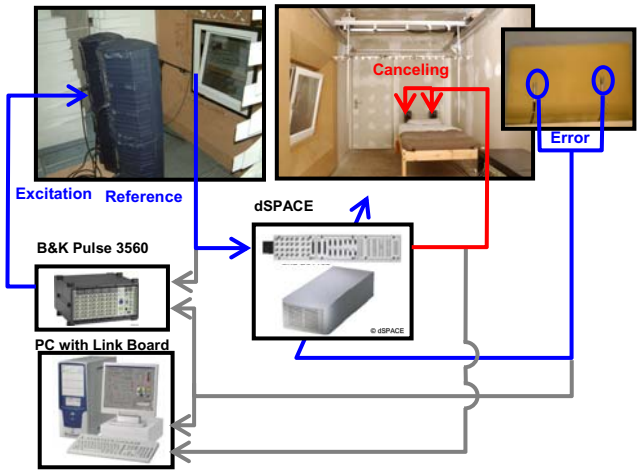

Figure 2: Experimental setup for real time testing of the active noise control system in a transmission test rig.

$$p_L(if) = P_{LX} q_p + S_{LL} q_{Ls} + S_{LR} q_{Rs}$$
$$p_R(if) = P_{RX} q_p + S_{RL} q_{Ls} + S_{RR} q_{Rs} \qquad \text{[Pa]} \qquad (1)$$

As shown by Equation (1), the complex pressures $p_L(if)$ and $p_R(if)$ at the left and right error microphone is determined by the transfer behaviour of the two primary paths $P_{LX}(if)$ and $P_{RX}(if)$ as well as by the transfer behaviour of the four secondary paths. The latter are defined by $S_{LL}(if)$, $S_{LR}(if)$, $S_{RL}(if)$ and $S_{RR}(if)$.

Physical Limit of Active Noise Reduction

As shown in [5] the performance of feed-forward ANC can be analyzed by frequency domain analysis of the residual error $e(if)$ at one of the error microphones. The relation between $S_{ee}(f)$, the (real valued) power spectra of the error signal in the controlled state, and $S_{dd}(f)$, the power spectra of the primary disturbance $d(if)$ in the uncontrolled state, measured at the same error sensor, is given by

$$S_{ee}(f) = \left(1 - \left|\gamma_{xd}(if)\right|^2\right) S_{dd}(f) \qquad [\mathrm{Pa^2}] \qquad (2)$$

with

$$\gamma_{xd}(if) := \frac{S_{xd}(if)}{\sqrt{S_{xx}(f) S_{dd}(f)}}, \qquad [1] \qquad (3)$$

where $S_{xx}(f)$ is the power spectrum of the reference signal and $S_{dx}(if)$ is complex cross spectral density between the disturbance measured at the error sensor and the reference signal. The noise reduction (NR) that can be achieved by an optimal controller can be calculated as follows

$$NR(f) = 10 \log_{10}\left(\frac{S_{ee}(f)}{S_{dd}(f)}\right). \qquad [\mathrm{dB}] \qquad (4)$$

Using a sample frequency of $f_s = 4096\,\mathrm{Hz}$ and frequency banded white noise ($80\,\mathrm{Hz} \le f \le 480\,\mathrm{Hz}$) as driving signal for the primary noise sources, coherence-analysis was performed for both error microphones. As in the desired application, the signal obtained by the reference microphone was used as reference.

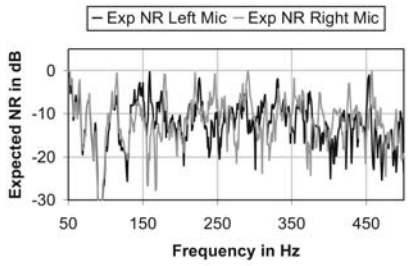

Figure 2: Noise reduction at error microphones estimated by coherence-analysis. Signal of reference microphone was used as reference for calculation of cross-spectral densities.

The NR calculated from Equation (4) is shown in Figure 2. It was found that for $80\,\mathrm{Hz} \le f \le 480\,\mathrm{Hz}$ a broadband NR of -17 dB / -18.0 dB can be expected at the left / right error microphone, if active feed-forward control is applied.

Description of Adaptive Control Scheme

To perform adaptive feed-forward control, an 1x2x2-implementation (one reference signal, two error signals, two adaptive controller) of the fast exact power normalized leaky filtered-x LMS algorithm, see [1], was implemented on a rapid prototyping system (Type: dSpace 1005).

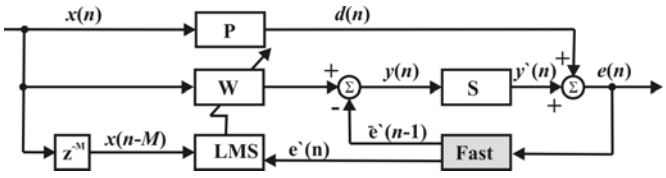

Figure 3: Schematic diagram of the fast exact power normalized leaky filtered-x LMS algorithm [4].

The implemented control scheme can be summarized as follows:

1. Perform recursive update of reference signal:

$$\begin{aligned}
&\textit{if}\ (n \cdot \bmod L = 0)\\
&\mathbf{x}(n) = \lambda \mathbf{x}(n-1) + \mathbf{a}(n-1)x(n) - \lambda \mathbf{b}(n-1)x(n-L)\\
&\textit{else}\\
&\mathbf{x}(n) = \mathbf{r}(n-1) + \mathbf{a}(n-1)\mathbf{x}(n) - \lambda \mathbf{b}(n-1)x(n-L)\\
&\textit{endif}\\
&\mathbf{a}(n) = \left[x(n-1)\ x(n-2) \cdots x(n-M+1)\right]^T\\
&\mathbf{b}(n) = \left[x(n-L)\ x(n-L-1) \cdots x(n-L+1-M)\right]^T,
\end{aligned} \qquad (5)$$

where $x(n)$ is the reference signal, M is the length of each finite impulse response (FIR) filter used to model the four secondary paths, L is length of the control filter, and λ is a leakage factor.

2. Compute controller output for the j = 1, 2 controller:

$$\begin{aligned}
y^{(j)}(n) &= \mathbf{x}^T(n)\mathbf{w}^{(j)}(n) - \mathbf{r}^T(n)\bar{\mathbf{e}}'^{(j)}(n-1)\\
\mathbf{x}(n) &= \left[x(n)\ x(n-1)\ \cdots x(n-M-L+1)\right]^T,
\end{aligned} \qquad (6)$$

where $\mathbf{w}^{(j)}(n)$ contains the L filter weights of the j-th controller and $\bar{\mathbf{e}}'^{(j)}$ contains the last L-1 filtered error signals according to Equation (7).

3. Update the error signal for the j = 1, 2 controller:

$$\begin{aligned}
\mathbf{e}'^{(j)}(n) &= \begin{bmatrix} 0 \\ \bar{\mathbf{e}}'^{(j)}(n-1) \end{bmatrix} + \Delta\mathbf{e}'^{(j)}(n)\\
\Delta\mathbf{e}'^{(j)}(n) &= \mu(n)\left[\mathbf{s}^{(1,j)}\ \mathbf{s}^{(2,j)}\right]\mathbf{e}(n),
\end{aligned} \qquad (7)$$

where $\mathbf{e}'^{(j)}$ contains the L filtered error signals at time step n, $\mathbf{s}^{(i,j)}$ is the FIR filter describing the impulse response between the i-th microphone and the j-th cancelling loudspeaker and $\mu(n)$ is the power normalized step size.

4. Update the filter weights of the j = 1,2 controller:

$$\mathbf{w}^{(j)}(n+1) = \nu \mathbf{w}^{(j)}(n) - \mathbf{x}(n-M)e'^{(j)}(n), \qquad (8)$$

where $\nu(n) = 1 - \gamma\mu(n)$ is the "common" leakage factor.

The algorithm given by Equation (5) – (8) produces the exact output signals and behavior than the standard power normalized leaky filtered-x LMS algorithm, see [1], but for an increase of components (reference or error microphones, cancelling loudspeakers), the computational complexity is decreased.

A schematic diagram of the implemented control scheme is shown in Figure 3. It clarifies that the block **Fast** includes a pre-filtering of the error signal $\mathbf{e}(n)$ as defined by Equation (7). The reference signal $x(n)$ is therefore delayed by M samples (the length of the plant model FIR filter).

Parameters of Active Control System

Real time testing of ANC systems requires the choice of proper values for fundamental parameters such as the sampling frequency f_s, the dimensionless step size $\alpha(n)$ and controller length L.

Effect of Sampling Frequency

In order to control frequencies up to 480 Hz, and to meet the Nyquist-Shannon criteria, the sampling rate was set to f_s = 4 kHz. Therefore, according to [2], the total system delay in the anti-aliasing filter, A/D converter, D/A converter, reconstruction filter, loudspeaker, plus the processing time of one sampling period T_s, was given by:

$$\delta_{T_s} \approx T_s\left(1+\frac{3}{8}N_p\right) = 0.00175\,\mathrm{s}\,, \tag{9}$$

where $N_p = 16$ is the number of poles in the anti-aliasing and reconstruction filters. Causality was ensured, because the minimum acoustic delay $\delta_{A_{\min}} \approx 0.0073\,\mathrm{s}$ between the secondary sources and the reference microphone was greater than δ_{T_s}.

As shown in [2], the choice of a certain sampling frequency also influences the damping that is obtained by the anti-aliasing and the reconstruction filters. Applying the formulas given in [2] aliasing was suppressed at $f_s/2$ by

$$R\log_2\left(\frac{f_s/2}{f_1}\right) \approx 93\,\mathrm{dB}\,, \tag{10}$$

where R = 45 dB/octave is the fall-off rate of the anti-aliasing filter, and $f_1 = 480\,\mathrm{Hz}$ is the bandwidth. Imaging effects where suppressed at $3f_s/4$ by

$$10 + R\log_2\left(\frac{3f_s/4}{f_1}\right) \approx 129\,\mathrm{dB}\,. \tag{11}$$

Specifying of Step Size

As also shown in [2], stability of the adaptive algorithm is ensured, if the normalized step size $\mu(n) = \alpha(n)/P_x(n)$ is bounded by

$$0 < \frac{\alpha(n)}{P_x(n)} < 2\frac{\mathrm{Re}[\lambda_m]}{|\lambda_m|^2}, \tag{12}$$

where $P_x(n)$ is the power of the reference signal, and λ_m is the m-th eigenvalue of $\left[\hat{\mathbf{R}}(n)^T\,\mathbf{R}(n)\right]$. The matrices $\mathbf{R}(n)$ and $\hat{\mathbf{R}}(n)^T$ are defined as

$$\mathbf{R}(n) = \begin{bmatrix} \mathbf{r}_1^T(n) & \mathbf{r}_1^T(n-1) & \dots & \mathbf{r}_1^T(n-M+1) \\ \mathbf{r}_2^T(n) & \mathbf{r}_2^T(n-1) & \dots & \mathbf{r}_2^T(n-M+1) \end{bmatrix} \tag{13}$$

$$\hat{\mathbf{R}}(n) = \begin{bmatrix} \hat{\mathbf{r}}_1^T(n) & \hat{\mathbf{r}}_1^T(n-1) & \dots & \hat{\mathbf{r}}_1^T(n-M+1) \\ \hat{\mathbf{r}}_2^T(n) & \hat{\mathbf{r}}_2^T(n-1) & \dots & \hat{\mathbf{r}}_2^T(n-M+1) \end{bmatrix} \tag{14}$$

with

$$\begin{aligned} \mathbf{r}_l(n) &= \left[r_{l1}(n)\;\; r_{l2}(n)\right]^T \\ \hat{\mathbf{r}}_l(n) &= \left[\hat{r}_{l1}(n)\;\; \hat{r}_{l2}(n)\right]^T. \end{aligned} \tag{15}$$

$\mathbf{r}_l(n)$ contains two reference signals at discrete time n, filtered by $\mathbf{s}^{(j,l)}$ that describes the (physical) response at the j-th error microphone due to an excitation of the l-th cancelling loudspeaker. As shown in Equation (15), $\hat{\mathbf{r}}_l(n)$ is defined in a similar manner by using $\hat{\mathbf{s}}^{(j,l)}$ that is the FIR filter model of the physical plant.

By analyzing Equation (12) and defining a minimum value of $\hat{P}_{x_{\min}} = 0.02\ \mathrm{V}^2$, an upper bound of $\alpha_{\max}$ = 0.02 was determined.

By using a safety factor of 0.1, see [4], the normalized convergence coefficient used for real time experiments was set to of α = 0.002, see [7].

Choice of Controller Length

Optimal control is realized, if the (remaining) error signal is uncorrelated to the filtered reference signal. To achieve this goal that is determined by the Wiener solution, the number of filter taps updated in the adaptive controller must be greater or at least equal to the number of filter weights that would be needed to identify the primary path, see [6].

If this is not the case, it is impossible to identify the primary path directly, and the optimal solution is only an optimal approximation to the impulse response on the primary path. The remaining error signal would therefore still be correlated to the reference signal.

In order to use a sufficient number of filter coefficients, the optimal length for the adaptive controller was estimated by quadratic optimization in time domain. Therefore, the cost function

$$J(n) = P_x^2\left\|\begin{pmatrix}\mathbf{p}_L\\ \mathbf{p}_R\end{pmatrix} + \begin{pmatrix}\hat{\mathbf{S}}_{LL} & \hat{\mathbf{S}}_{LR}\\ \hat{\mathbf{S}}_{RL} & \hat{\mathbf{S}}_{RR}\end{pmatrix}\begin{pmatrix}\mathbf{w}_1\\ \mathbf{w}_2\end{pmatrix}\right\|_2^2 = \min!\,, \tag{16}$$

where $\mathbf{p}_L, \mathbf{p}_R$ are the $(L\times 1)$ matrices containing the (discrete) impulse response functions of the primary path and $\hat{\mathbf{S}}_{IJ}$ are $(L+M-1\times L)$ matrices containing the plant models of the secondary paths, was minimized with respect to the unknown filter weights ordered in the $(L\times 1)$ column matrices $\mathbf{w}_1$ and $\mathbf{w}_2$, see [3].

It was found that a controller length of 1024 taps is sufficient to de-correlate the error signals from the reference signal, see [3] and [7].

Performance of Control System

To determine the real time performance of the ANC system, the transmission test rig was excited by frequency banded white noise $80\,\text{Hz} \le f \le 480\,\text{Hz}$.

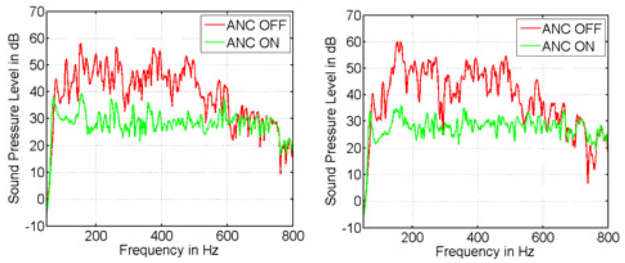

Figure 4: Sound pressure level at left (look left) and right (look right) error microphone for the controlled and the uncontrolled state. System was excited with frequency banded white noise 80 Hz $< f <$ 480 Hz.

As shown in Figure 4, the primary disturbance was significantly reduced by the adaptive control scheme. A total NR of -18 dB was obtained at the left error microphone and a total NR of -17 dB at the right error microphone, respectively. Comparing these results with the values estimated with Equation (4), it can be concluded that the physical limits of NR were achieved.

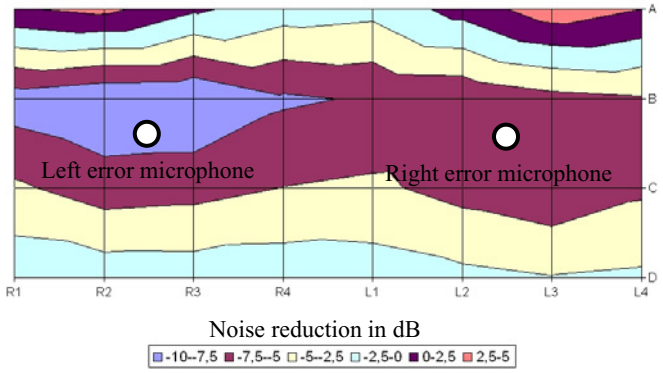

Figure 5: Map of noise reduction due to active control measured 8 cm above the pillow for broadband excitation with 80 Hz $< f <$ 480 Hz. Distance between the grid points is 10 cm. Error microphones were not used for interpolating of data.

To give an impression on the effect of ANC in the neighbourhood of the error microphones, the sound field was mapped 8 cm above the pillow using a microphone array with a spacing of 10 cm between each sensor. The control profit measured at 32 positions is shown in Figure 5 using a linear interpolation between the measurement points. The results indicate that for practical application a -10 dB zone of quiet has to be realized, at least for the region BC-R1L4.

A comparison between an optimal controller response, calculated by quadratic optimization in frequency domain, and the steady state controller response of the converged ANC system is shown in Figure 6. It can be seen that below 250 Hz, the adaptive controller is capable of reproducing the (theoretically) optimal solution. Above 250 Hz, however, this is not the case.

As shown in Figure 4, the controller whites the error spectra. It must therefore be concluded that the difference between the optimal controller response and the controller response obtained at steady state is caused by uncorrelated noise.

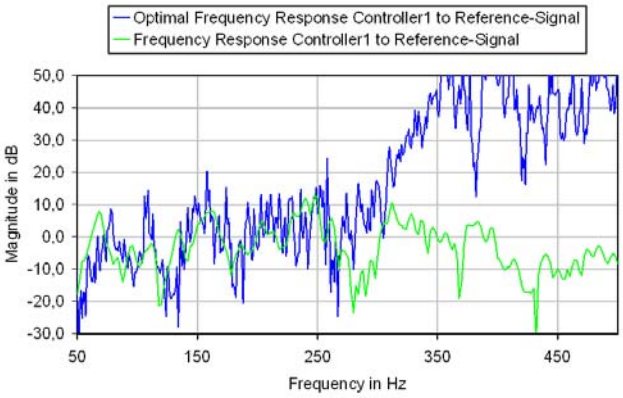

Figure 6: Comparison of optimal controller response and controller response measured in the steady state of converged controller for broadband excitation with frequency banded white noise 80 Hz $< f <$ 480 Hz.

Summary

A functional model of an active noise control system for bedrooms integrated in a transmission test rig was analyzed. It was found that the physical limits of the controller performance can be reached, if the real time processor is capable of processing sufficient filter lengths. The use of an outdoor microphone that was not affected by the indoor secondary sources was adequate to measure a proper reference signal. It was also found that the active noise control system was capable of generating a zone of quiet in the neighbourhood of the error microphones. Future work will be focussed on the enlargement of the zone of quiet as well as on the robustness of the active control system.

References

[1] Douglas, S., C.: Fast exact filtered-X LMS and LMS algorithms for multichannel active noise control. IEEE Int. Conf. Acoust., Speech, Signal Processing, Munich, Germany, Vol. **1** ,(1997) pp. 399-402

[2] Elliott, S.: Signal processing for active noise control. Academic press, San Diego (2001)

[3] Holters, M., Zölzer, U.: Unterauftrag zum Forschungsvorhaben Aktive Lärmminderung in Wohn- und Schlafräumen, DBU-Az: 24483, (2008)

[4] Kochan, K., Kletschkowski, T., Sachau, D., Breitbach, H.: Active noise control in a semi-closed an aircraft. ISMA '08 – Int. Conf. on Noise and Vibration Engineering, (2008), Leuven, Belgium, Sept. 15 – 17

[5] Kou M., S., Morgan D., R.: Active noise control systems – Algorithms and DSP implementations. John Wiley & Sons Inc, New York, 1996

[6] Moschytz, G., Hofbauer, M.: Adaptive Filter. Springer, Berlin, (2000)

[7] Sachau, D., Kletschkowski, T., Simanowski, K.: Aktive Lärmminderung in Wohn- und Schlafräumen, DBU-Az: 24483, (2008)